small NANO MICRO

Stretchable Electronics

Stretchable, Wireless Sensors and Functional Substrates for Epidermal Characterization of Sweat

*Xian Huang, Yuhao Liu, Kaile Chen, Woo-Jung Shin, Ching-Jui Lu, Gil-Woo Kong, Dwipayan Patnaik, Sang-Heon Lee, Jonathan Fajardo Cortes, and John A. Rogers**

This paper introduces materials and architectures for ultrathin, stretchable wireless sensors that mount on functional elastomeric substrates for epidermal analysis of biofluids. Measurement of the volume and chemical properties of sweat via dielectric detection and colorimetry demonstrates some capabilities. Here, inductively coupled sensors consisting of LC resonators with capacitive electrodes show systematic responses to sweat collected in microporous substrates. Interrogation occurs through external coils placed in physical proximity to the devices. The substrates allow spontaneous sweat collection through capillary forces, without the need for complex microfluidic handling systems. Furthermore, colorimetric measurement modes are possible in the same system by introducing indicator compounds into the depths of the substrates, for sensing specific components (OH^-, H^+, Cu^+, and Fe^{2+}) in the sweat. The complete devices offer Young's moduli that are similar to skin, thus allowing highly effective and reliable skin integration without external fixtures. Experimental results demonstrate volumetric measurement of sweat with an accuracy of 0.06 $\mu L/mm^2$ with good stability and low drift. Colorimetric responses to pH and concentrations of various ions provide capabilities relevant to analysis of sweat. Similar materials and device designs can be used in monitoring other body fluids.

1. Introduction

Emerging wearable sensor technologies offer attractive solutions for continuous, personal health/wellness assessment,[1,2] forensic examination[3] patient monitoring[4,5] and motion recognition.[6,7] Recent advances in epidermal electronics[8] provide classes of skin-mounted sensors and associated electronics in physical formats that enable intimate, conformal contact with the skin. The soft, non-irritating nature of this contact yields an interface that simultaneously provides high precision, accurate measurement of biophysiological parameters, such as temperature,[9] hydration,[10] strain,[11] and biopotential.[12] Such epidermal sensors are ultrathin, breathable and stretchable, with mechanical and thermal properties that closely match to the skin itself, to enable effective skin integration with minimum constraints on natural processes. The results provide unique capabilities in long-term, reliable health monitoring.

An important measurement mode in such devices may involve the analysis of body fluids (blood, interstitial fluid, sweat, saliva, and tear), to gain insights into various aspects of physiological health.[13–16] Such function in wearable sensors, generally, and epidermal electronics in particular, is relatively unexplored. Existing devices either use complex microfluidic systems for sample handling[17–20] or involve purely concentration-based measurement without sample collection and storage, or access to parameters related to

Dr. X. Huang, Y. Liu, K. Chen, W.-J. Shin, C.-J. Lu, G.-W. Kong, D. Patnaik, S.-H. Lee, J. F. Cortes, Prof. J. A. Rogers
University of Illinois at Urbana-Champaign
Frederick Seitz Materials Research Laboratory
104 S. Goodwin Ave, Urbana, IL 61801, USA
E-mail: jrogers@illinois.edu

DOI: 10.1002/smll.201400483

quantity and rate.[21–23] In addition, mechanical fixtures, straps and/or tapes that are typically required to maintain contact of these devices with the skin do not lend themselves well to continuous, long term monitoring without discomfort.[24] In the following, we report a set of materials and device architectures that provide advanced capabilities in this area. The key concept involves the use of functional soft substrates to serve as a means for microfluidic collection, analysis and presentation to co-integrated electronic sensors and/or external camera systems. The pores of these substrates spontaneously fill with body fluids that emerge from the skin, where they induce colorimetric changes in the substrate and alter the radio frequency characteristics of integrated electrical antenna structures. The results offer valuable insights into the properties and volume of sweat, and their relationships to fluctuations in body temperature,[25] fluid and electrolyte balance,[26] and disease state.[27] The devices also eliminate the need for direct skin-electrode contacts, thereby minimizing irritation that can be caused by contact between the skin and certain metals,[28] while at the same time enabling repeated use of a single device with minimal noise induced by motion artifacts. The sensors exploit inductive coupling schemes, without on-chip detection circuits but with some potential for compatibility using near-field communication systems that are found increasingly in portable consumer electronic devices. The entire sensing system offers flexible and stretchable mechanics, with form factors that approach those of epidermal electronics.

2. Results and Discussion

Figure 1a shows images and schematic illustrations of a typical device (22×28 mm^2 for the surface area of the substrate, and 10×15 mm^2 for the dimension of the sensor) that includes an inductive coil and a planar capacitor formed with interdigitated electrodes. The coil consists of four turns of thin copper traces in a filamentary serpentine design that affords both flexibility and stretchability. The width of the trace is 140 μm, and the lengths of the inner and outer turns are 4.8 and 9.5 mm, respectively. The electrodes consist of serpentine wires (50 μm in width) that have lengths between 6.5 to 8.4 mm, to form 9 digits with a digit-to-digit spacing of 600 μm. The dielectric properties of the microporous supporting substrate strongly influence the capacitance of the structure.

In this way, the sweat sensor enables capacitive detection of the change of the dielectric properties of the substrate as its pores fill with biofluids (e.g. sweat). An external primary coil generates a time varying electromagnetic field that induces a current flow within the sensor. The impedance of the sensor is then determined by the amount of sweat within the substrate; this impedance influences that of the primary coil placed in proximity to the device. The resonance frequency (f_0) of the sensor can be determined from the frequency of a phase dip (or a peak in the phase difference, $\Delta\theta$, obtained from the subtraction of the phase of the primary coil with and without the sensor underneath) in the phase-frequency spectrum of the primary coil.[29–32] At measurement frequencies examined here (100 to 200 MHz), free water molecules

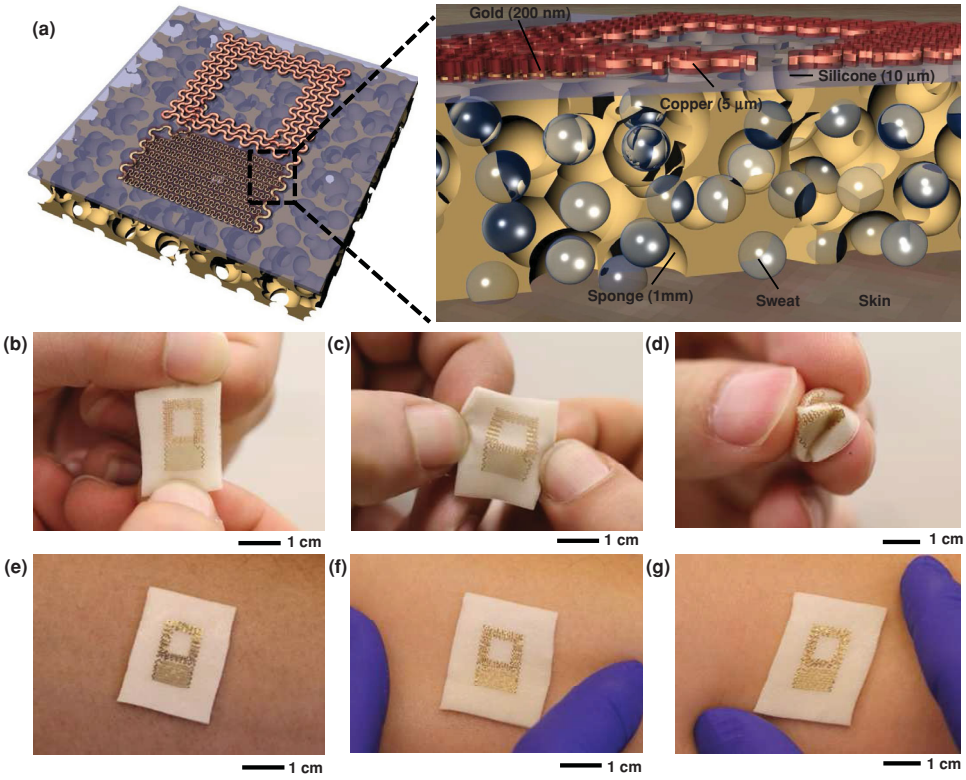

Figure 1. (a) Schematic illustration of a passive wireless capacitive sensor designed for sensing of sweat from the surface of the skin. Pictures of a device in (b) longitudinal and (c) latitudinal states of deformation, and crumpled between the fingers (d). Pictures of a device mounted on the skin in (e) undeformed, (f) uniaxially stretched and (g) biaxially stretched configurations.

NANO MICRO small

are under the influence of δ relaxation.[33] The response of the functional polymer substrates only involve contributions from induced charges. The movement of the water molecules and dynamics of the induced charges are sufficiently fast to respond to the external electromagnetic field. As a result, the combined dielectric properties of substrate and the sweat exhibit an invariant dielectric response over a wide range of frequencies (Figure S1a). For present purposes, the frequency-dependence in the dielectric properties of the substrate can be ignored.

The sensor offers mechanical properties (elastic modulus≈80 kPa) similar to those of the skin.[34] The thickness of the substrate (1 mm), along with its lateral dimensions and porosity define the amount of fluid that it can capture. The devices exhibit robust, elastic behavior under axial stretching (Figure 1b and 1c) and other more complex modes of deformation (Figure 1d). Attachment of the sensor onto the skin (Figure 1e) using a thin layer of commercial spray-on bandage as adhesive leads to reversible skin/sensor bonding that can withstand significant extension and compression of the skin with sufficient mechanical strength to prevent delamination (Figure 1f and 1g).

In vitro experiments involve slow introduction of 0.6 mL of buffer solution (phosphate buffered saline, Sigma-Aldrich Corporation, St. Louis, Mo, USA) onto the substrates with a syringe pump, over the course of ≈40 minutes (**Figure 2**d). The resonance frequency of the sensor (f_0), as measured by the shift of the phase peak of a primary coil placed in proximity to the device (Figure 2c), decreases with increasing buffer solution content in the substrate. This response reflects increases in the permittivity due to replacement of air with buffer solution in the pores of the substrate, leading to an increase in the capacitance of the interdigitated electrodes associated with their proximity to the substrate. For a typical porous polyurethane (PUR) (PUR permittivity = 7,[35] PUR substrate permittivity = 1.42 at 0.93 porosity in air) (Figure 2a), f_0 shifts from 195.3 to 143.3 MHz in this experiment (Figure 2d). Drying of the sensor in air at room temperature leads to the recovery of f_0, eventually to the original value (195.3 MHz) over a period of ≈6 hours, indicating a reversible response with relative insensitivity to residual salt that might remain in the substrate.

Assessment of performance with human subjects involves use of sensors on cellulose paper (CP) and silicone substrates attached to the arms of two volunteers. Reference substrates made of the same materials with similar sizes placed in close proximity to the sensors provide means for determining the accuracy and establishing a calibrated response (Figure 2b). The monitoring includes measuring the value of f_0 of the sensors and the weight of the reference substrates every 5 min for a period of 2 hours. The results indicate that f_0 is inversely proportional to the weight of the reference sensor, such that the response can be calibrated with any two measured weights. The calibrated results closely follow weight changes of 0.4 (Figure 2e) and 0.2 g (Figure 2f) in the reference substrates, corresponding to 0.4 and 0.2 mL of sweat over the sensing areas.

Dimensional changes associated with deformation of the skin or swelling of the device caused by sweat absorption could, conceivably, lead to changes in f_0. Strain induced effects can be examined by biaxially stretching a device and measuring f_0 at various states of deformation (Figure S2a). The results show changes of only ≈0.9 MHz for biaxial strains of 27% (Figure 2g) that are comparable to those caused by the absorption of water (Figure S2b). The modest changes in f_0 under biaxial stretching may be attributed to the symmetric design of the sensor coil as well as mutual compensation of the changes in lengths and spacings of the interdigitated electrodes. We note that the effects of temperature are also small. In particular, data indicate (Figure S1b) that f_0 shifts from 199.25 MHz to 196.63 MHz when the temperature is changed from 25 to 45 °C. Finally, although the salinity and ionic content of the sweat may lead to changes in both conductivity and permittivity, experiments with buffer solutions having various concentrations of sodium chloride (0 to 4.5 g/L) reveal only small variations in f_0 (≈0.6 MHz; Figure 2h).

The sensors exhibit excellent repeatability and are suitable for repeated use. Multiple (i.e. five) measurements using sensors on CP and silicone substrates serve as demonstrations. Between each measurement, immersion in water followed by drying on a hot plate regenerates the devices. The changes in f_0 are repeatable for experiments that involve injection of 0.6 mL buffer solution (Figure 2i and S1c). The average change in f_0 is 58.3 MHz with a standard deviation of 1.1 MHz for the sensor on CP; the corresponding values for silicone are 60.1 MHz and 3.6 MHz, respectively. The changes in f_0 undergo different temporal patterns, as might be expected due to the differences in chemistry, microstructure and pore geometry for these two substrates. Measurements over 3 hours show no drifts in f_0 (Figure S1d). The noise levels are <0.7 MHz; this parameter, together with an average change of f_0 of 58.3 to 60.1 MHz for 0.6 mL buffer solution over a surface area of 22×28 mm^2, suggests a measurement accuracy of ≈0.06 mL/mm^2.

The coil structures can be mounted onto various types of functional substrates. Demonstrated examples include recycled cellulose sponge (RCS), polyurethane sponge (PUR), polyvinyl alcohol sponge (PVAS), cellulose paper (CP), and silicone sponge (**Figure 3**a). Cutting with a hot-wire device (PUR, silicone) or with a razor blade (other) yields the appropriate lateral dimensions and thicknesses. Spin-coated silicone films with accurately controlled thickness (≈10 μm; Figure 3b) enable strong bonding between each of these functional substrates and the sensors through surface chemical functionalization, while preventing direct contact between the sensors and the sweat. Relative characteristics in water absorption are also important to consider, as described in the following.

The percentage gain in weight of the various porous materials after immersion in water defines their ability to hold fluids; the results are ≈2300% (RCS), ≈1200% (PUR), ≈750% (PVAS), ≈350% (CP), and ≈1500% (silicone) (Figure 3c). These data, together with measured volume changes yield the porosity levels: 0.97 (RCS), 0.93 (PUR), 0.90 (PVAS), 0.83 (CP) and 0.95 (silicone) (Figure 3d). The water permeability can be determined from the capillary water absorption rate by combining Darcy's law[36] and the Hgaen-Poiseuille equation.[37] Strips of the substrates (3 mm in width and 28 mm

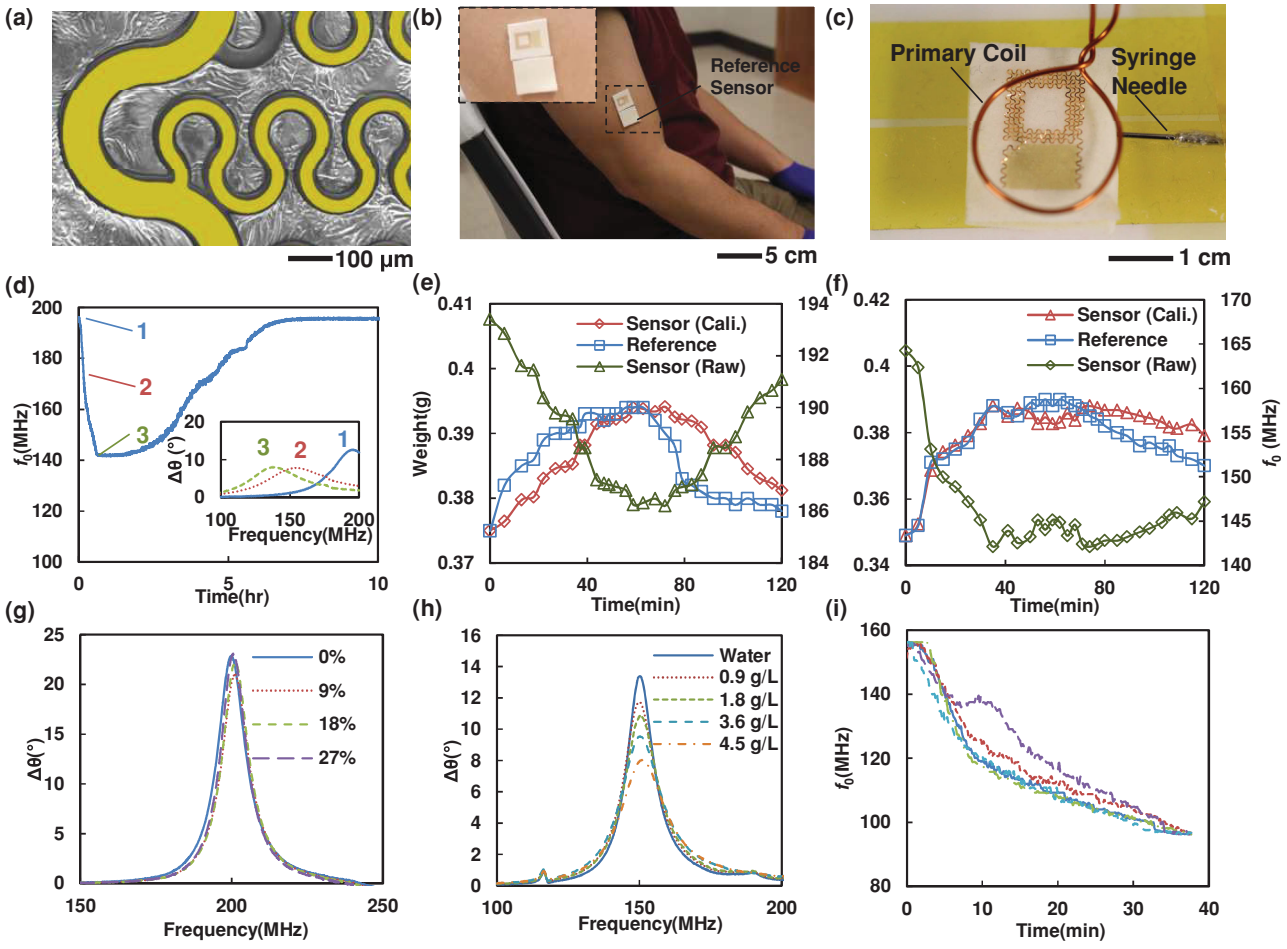

Figure 2. (a) Scanning electron micrograph of a sensor on a PUR substrate coated with a thin silicone film; the regions colorized in yellow represent the interdigitated gold electrodes. (b) Picture of a sweat sensor and a reference sensor on the arm of a volunteer for *in-vivo* testing. (c) Picture of a sweat sensor underneath a primary coil. A syringe needle inserted into the sensor delivers controlled amounts of a buffer solution through a syringe pump. (d) Representative data showing the response of the sensor (resonant frequency, f_0) as a function of time after introduction of 0.6 mL buffer solution (labeled 1). The initial response (labeled 2) corresponds to wicking of the solution into the porous substrate, to yield a stable overall shift in f_0 (labeled 3). As the solution evaporates over the next several hours, f_0 recovers to approximately the initial value. The inset shows the phase difference measured by the primary coil at the three time points indicated in the main frame. (e, f) Results of testing on two volunteers, with comparisons to changes in weight evaluated using similar porous substrates (without detection coils) placed next to the sensors. Both f_0 and the weight of the sensors calibrated from f_0 are shown, along with comparison to the weight of the reference substrates. (g) Phase response of a sensor under biaxial strain from 0 to 27%. (h) Phase response as a function of concentration of sodium chloride, from 0 to 4.5 g/L. (i) Change in f_0 of a sweat sensor on a CP substrate as a function of time during controlled injection of 0.6 mL buffer solution.

in length) are partially immersed into water with red dye (3 mm under the water). A camera enables measurements of changes in height of the absorbed water as a function of time (Figure 3e). The CP material exhibits the fastest absorption rate (complete filling in ≈6 s), followed by the RCS (≈25 s). The PUR shows the smallest rate, with an increase in height of 8.3 mm over 130 s (Movie S2). These rates depend strongly on the pore size and degree of interconnectedness and on the contact angle. The latter can be determined optically (Figure S3b); the former can be obtained by scanning electron microscopy (Figure S3a) or by calculation and measurement of the height of absorbed water at a long period of time (details in supporting information). The permeability of the five substrates are 2.4 (RCS), 0.3 (PUR), 0.4 (PVAS), 8.7 (CP), and 8.6 (silicone) μm^2 (Figure 3f).

In addition to dielectric response, absorption of water changes both the transparency, due to index matching effects, and the overall dimensions, due to swelling (**Figure 4**a and 4c). These effects can be used as additional measurement parameters to complement the electrical data described previously. The optical behavior can be illustrated by placing a sensor on a region of the skin with a temporary tattoo pattern. Continuous introduction of a buffer solution, up to a total of 0.6 mL, leads to increasing levels of transparency. Selected regions of the images in Figure 4a can be used to obtain RGB (red, green, and blue) intensities at different locations. The resulting data (Figure 4b) indicate that the water content is inversely proportional to the ratio of the RGB intensity on the sensor and the skin. The water also induces changes in the lateral dimensions. These changes

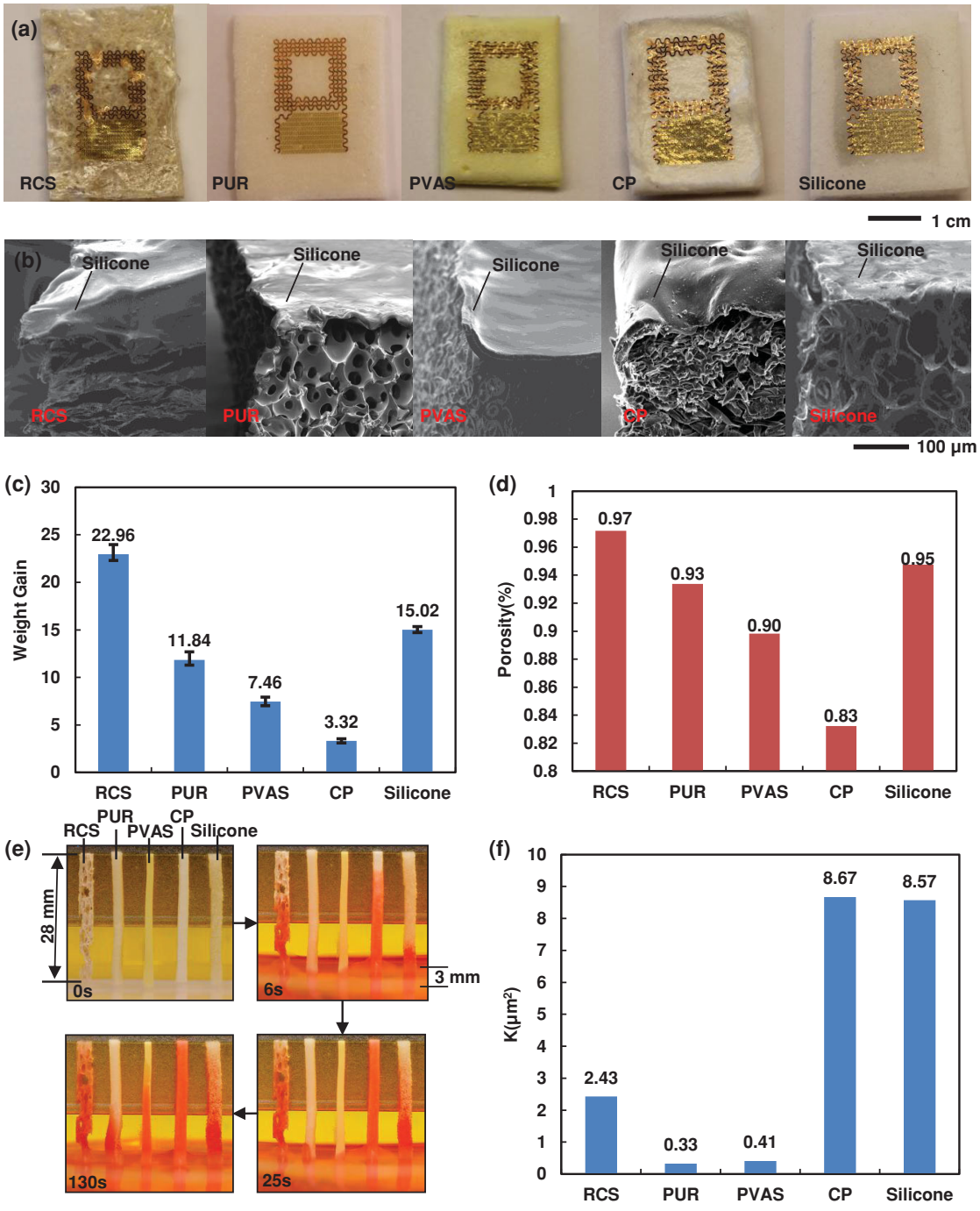

Figure 3. (a) Wireless sweat sensors based on different porous substrates. (b) SEM images of the substrates coated with thin layer of silicone to facilitate chemical bonding between the sensors and the substrates. (c) Weight gain of different substrate materials associated with immersion in water. (d) Porosity of the substrate materials. (e) Images of strips of the substrate materials when partially immersed into water with red dye. (f) Water permeability of the substrate materials.

can be measured by optically tracking the displacements of an array of opaque dots (Cr, by electron beam evaporation through a shadow mask) on the device (Figure 4c). The results indicate a large displacement response to introduction of 0.2 mL of the buffer solution (≈2.3 mm dot displacement), but with diminishing response for an additional 0.4 mL (≈0.5 mm dot displacement). Nevertheless, these motions, which may be limited by mechanical constraints associated with mounting on the skin, might have some utility in measuring sweat loss.

The substrates can be rendered more highly functional, from an optical standpoint, by introduction of chemicals or immobilized biomolecules. Resulting interactions with the sweat can be evaluated through electrical dielectric measurement or simply colorimetric detection. For example, silicone substrates doped with colorimetric indicators render

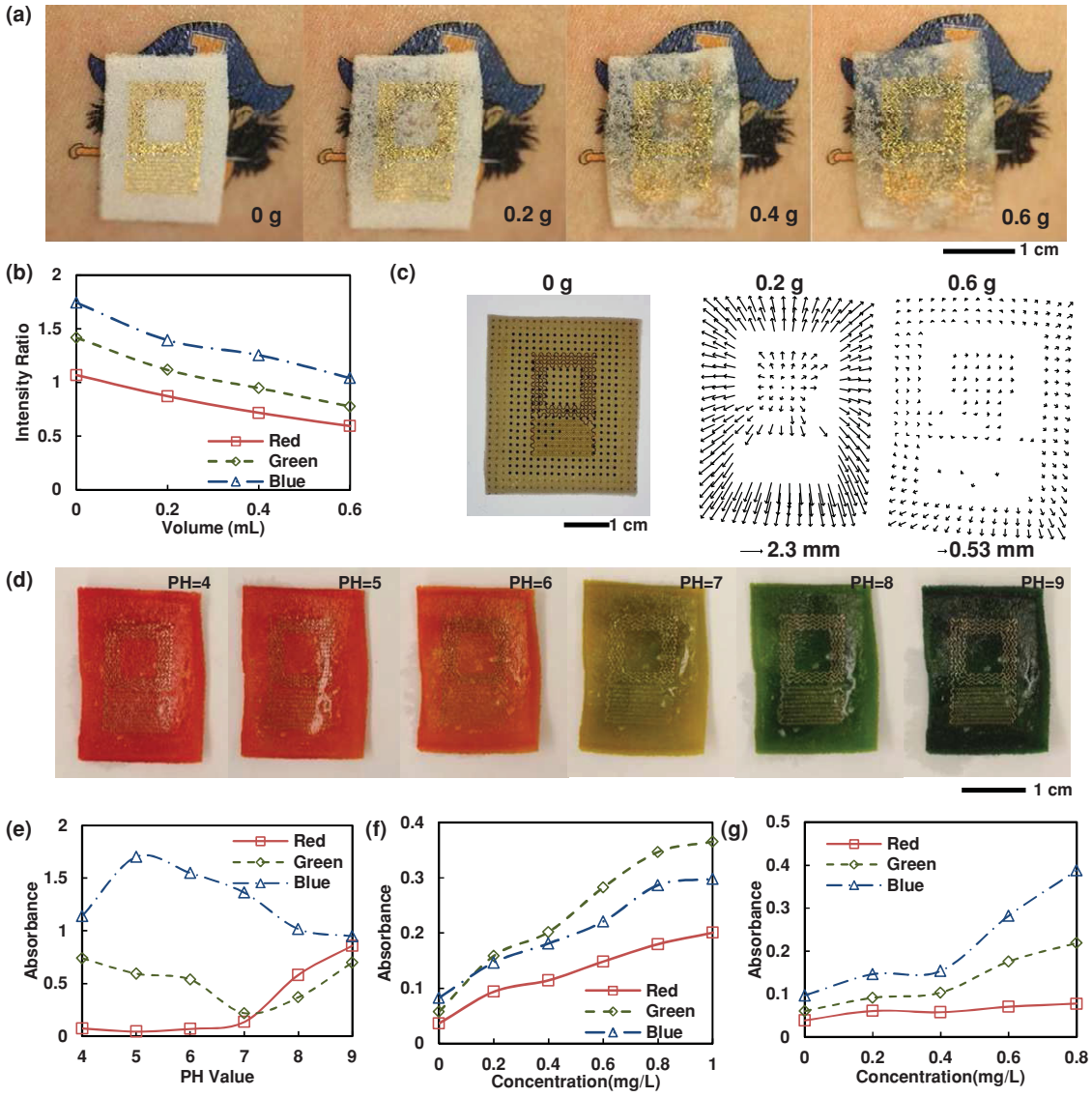

Figure 4. (a) Images that illustrate a simple colorimetric detection scheme, based on systematic increases in transparency with water absorption. (b) The ratio of RGB intensity for a sensor like the one illustrated in (a), as a function of water absorption. (c) An image and vector diagrams corresponding to a sensor and its expansion due to water absorption. (d) Series of pictures of a sensor doped with a pH indicator, each collected with absorbed water at a different pH value. (e) Absorbance of RGB channels at different pH values. (f) Absorbance of RGB channels at different copper concentrations. (g) Absorbance of RGB channels at different iron concentrations.

sensitivity to relevant biophysical/chemical parameters, such as pH values (Figure 4d), free copper concentrations (Figure S4a), and iron concentrations (Figure S4b). To demonstrate pH detection, standard buffer solutions with pH values from 4 to 9 are introduced into a substrate that is dyed with a mixture of several different pH indicators (bromothymol blue, methyl red, Methyl yellow, thymol blue, and phenolphthalein). These chemicals reversibly react with free –OH groups and/or protons in the buffer solutions, leading to changes in absorption spectra. Accordingly, the substrate undergoes a series of color changes that reveal the pH values (Figure 4d). In addition, buffer solutions with copper (Figure S4a) and iron (Figure S4b) at physiological concentrations (0.8 to 1 mg/L) can also be detected using similar colorimetric schemes. The intensities of individual colors (red, green, and blue) extracted from the images determine changes in analyte concentrations (Figure 4e, 4f and 4g). This type of strategy has potential utility when used in combination with the sorts of wireless schemes introduced here. For example, near field communication[38] enabled devices such as cellphones also offer digital image capture capabilities, for simultaneous colorimetric measurement.

3. Conclusion

The results presented here provide materials and design strategies for integrating flexible and stretchable wireless sensors on functional substrates. Demonstrated devices intimately mounted on the skin enable non-invasive, wireless quantification of sweat loss as well as colorimetric detection of sweat composition. Similar strategies can be used to

develop sensors for monitoring a range of key parameters associated not only with sweat but with other body fluids.

4. Experimental Section

To fabricate the device, a layer of polydimethylsiloxane (PDMS, 20 μm thick) is first spin-coated onto a glass slide (Figure S5a). Curing the PDMS at 120 °C for 10 min and treating its surface with reactive ion etching (RIE) for 5 min (20 sccm O_2, 300 mTorr pressure, 150 W power) allows conformal spin-coating of a layer of polyimide (PI; 1 μm thick) on top. A bilayer of chrome (5 nm) and gold (200 nm) deposited by electron beam (ebeam) evaporation is photolithographically patterned to form serpentine interdigitated electrodes (Figure S5b). An additional spin-coated PI (1 μm) electrically insulates the surfaces of the electrode patterns, while selective regions on the PI layer is etched by RIE for electrical contact between the electrode and serpentine coils formed by patterning a layer of ebeam deposited copper (6 μm) (Figure S5c). The entire patterns are encapsulated by another spin-coated PI layer (1 μm). Patterned RIE yields an open mesh layout, capable of release onto the surface of a target substrate by use of water-soluble tape (Aquasol ASWT-2, Aquasol Corporation, North Tonawanda, NY, USA). To prepare the functional substrates, a layer of uncured silicone (10 μm thick) is spin-coated onto a water soluble tape fixed on its edges to a glass slide by Scotch tape. Pre-curing the silicone at 150 °C for 1 min transforms the liquid precursor into a tacky, soft solid (Figure S5e). Placing the substrates on the silicone film with gentle pressure allows the partially cured film to crosslink with porous structures on the surface. The silicone and the substrates are then fully cured at 120 °C to achieve robust bonding (Figure S5f). The resulting structure is removed from the glass, and rinsed with water to remove the water soluble tape. Deposition of Ti/SiO_2 (5/60 nm) onto the exposed backside of the sensor facilitates chemical bonding to the PDMS film on the functional substrates after UV ozone activation. Dissolving the water soluble tape yields an integrated device with excellent levels of mechanical stretchability and flexibility (Figure S5g and Figure 1b). The functional substrates can be immersed into colorimetric indicators, followed by baking at 100 °C on a hotplate to dry the devices.

Five hydrophilic porous substrates serve as the sweat absorption materials, including Whatman GB003 cellulose paper (GE Healthcare Life Sciences, Pittsburgh, PA, USA), Scotch-Brite recycle cellulose sponge (3M Cooperation, St. Paul, MN, USA), polyvinyl alcohol sponge (Perfect & Glory Enterprise Co., Ltd., Taipei), Kendall hydrophilic polyurethane foam dressing (Covidien Inc., Mansfeld, MA, USA), and Mepilex silicone foam dressing (Mölnlycke Health Care AB, Sweden). For colorimetric detection, a universal pH indicator (pH 2–10) (Ricca Chemical, Arlington, TX, USA) yields responses to buffer solutions with well-defined pH (Sigma-Aldrich Corporation, St. Louis, Mo, USA). Colorimetric copper and iron ion detection is enabled by a copper color disc test kit (CU-6, Hach Company, Loveland, Colorado, USA) and an iron color disc test kit (IR-8, Hach Company, Loveland, Colorado, USA), while standard stock solutions of copper and iron (Hach Company, Loveland, Colorado, USA) are diluted to achieve different ion concentrations.

The sensors can be integrated onto the skin using a process as shown in the movie in the supporting information (Movie S1). Briefly, spray bandage (Nexcare No Sting Liquid Bandage Spray, 3M Cooperation, St. Paul, MN, USA) is first applied onto the corresponding skin region. Evaporation of the solvent results in a tacky, water-permeable film that does not significantly influence the transdermal water loss from the skin and provides sufficient adhesion to fix the sweat sensors onto the skin. The sensor is then applied to the skin with continuous pressure over several seconds. The bonding is reversible, but is sufficiently strong to accommodate heavy sweating and shear forces.

The electrical reponses of the sensors are evaluated using a HP 4291A impedance analyzer (Agilent Technologies, Santa Clara, CA, USA) with a frequency range from 1 MHz to 1.8 GHz. The analyzer connects to a one-turn hand-wound copper primary coil whose resonance frequency is significantly different from the sweat sensor. The coil is placed 2 mm away from the sweat sensor during the measurement. However, small variations in the distance between the coil and the sweat sensor are tolerable, with negligible effects on the results. A xyz mechanical stage and a rotational platform allow manual adjustment of the position and orientation of the primary coil relative to the sweat sensor. The primary coil provides a time varying electromagnetic field that induces alternating voltages in the sweat sensor. Changes of sweat content within the substrate of the sensor lead to changes in the capacitance of the sweat sensor and its f_0. A syringe pump (KD Scientific Inc., Holliston, MA, USA) is used to deliver buffer solutions to the sensors during the in vitro experiments. The sweat sensors with a CP substrate and a silicone porous material are mounted on the arms of two volunteers for 2 hour in vivo testing, with reference substrates of the same materials and sizes placed in close proximity to the sweat sensors (Figure 2b). For the first hour, the volunteers exercise continuously to generate sweat, and then stop to rest for the second hour. During the measurement, the sweat sensors remain on the skin, while the reference sensors are peeled off every 5 min to record their weight using a precise balance and reattached back to the same positions afterwards.

The absorbance values are estimated from the digital images by accessing the RGB (red, green, blue) values of the selected regions on the experimental images using ImageJ.[39] The average RGB values are determined from multiple pixels enclosed within a rectangular frame drawn by ImageJ with a plugin called, "measure RGB". The Absorbance (A) defined as the negative log of the transmittance (I_n/I_{blank}), is then calculated using the following formula:

$$A = -\log(I_n/I_{blank}) \quad (1)$$

in which I_n denotes the R, G or B values for the functional substrates and I_{blank} the R, G, or B value for the background, both obtained from the experimental images.

Supporting Information

Supporting Information is available from the Wiley Online Library or from the author.

Acknowledgements

We would like to acknowledge support from MC10, Inc. and the Gates Foundation. This work was conducted in the Frederick Seitz

Materials Research Laboratory Central Facilities, University of Illinois at Urbana-Champaign.

[1] M. Chan, EstC, J.-Y. Fourniols, C. Escriba, E. Campo, *Artif. Intell. Med.* **2012**, *56*, 137.
[2] A. Lay-Ekuakille, S. Mukhopadhyay, A. Lymberis, in *Wearable and Autonomous Biomedical Devices and Systems for Smart Environment*, Vol. *75*, Springer, Berlin Heidelberg, 237.
[3] A. J. Bandodkar, A. M. O'Mahony, J. Ramirez, I. A. Samek, S. M. Anderson, J. R. Windmiller, J. Wang, *Anal.* **2013**, *138*, 5288.
[4] P. Bonato, *IEEE Eng. Med. Biol. Mag.* **2010**, *29*, 25.
[5] P. M. Deshmukh, C. M. Russell, L. E. Lucarino, S. N. Robinovitch, Enhancing clinical measures of postural stability with wearable sensors, presented at *Engineering in Medicine and Biology Society (EMBC), 2012 Annual International Conference of the IEEE*, Aug. 28 2012-Sept. 1 2012.
[6] J. Varkey, D. Pompili, T. Walls, *Pers. Ubiquit. Comput.* **2011**, *16*, 897.
[7] J. R. Windmiller, J. Wang, *Electroanal.* **2013**, *25*, 29.
[8] D.-H. Kim, N. Lu, R. Ma, Y.-S. Kim, R.-H. Kim, S. Wang, J. Wu, S. M. Won, H. Tao, A. Islam, K. J. Yu, T.-i. Kim, R. Chowdhury, M. Ying, L. Xu, M. Li, H.-J. Chung, H. Keum, M. McCormick, P. Liu, Y.-W. Zhang, F. G. Omenetto, Y. Huang, T. Coleman, J. A. Rogers, *Science* **2011**, *333*, 838.
[9] R. C. Webb, A. P. Bonifas, A. Behnaz, Y. Zhang, K. J. Yu, H. Cheng, M. Shi, Z. Bian, Z. Liu, Y. S. Kim, W. H. Yeo, J. S. Park, J. Song, Y. Li, Y. Huang, A. M. Gorbach, J. A. Rogers, *Nat. Mater.* **2013**, *12*, 938.
[10] X. Huang, H. Cheng, K. Chen, Y. Zhang, Y. Liu, C. Zhu, S. C. Ouyang, G. W. Kong, C. Yu, Y. Huang, J. A. Rogers, *IEEE Trans. Biomed. Eng.* **2013**, *60*, 2848.
[11] N. Lu, C. Lu, S. Yang, J. Rogers, *Adv. Funct. Mater.* **2012**, *22*, 4044.
[12] W.-H. Yeo, Y.-S. Kim, J. Lee, A. Ameen, L. Shi, M. Li, S. Wang, R. Ma, S. H. Jin, Z. Kang, Y. Huang, J. A. Rogers, *Adv. Mater.* **2013**, *25*, 2773.
[13] K. Virkler, I. K. Lednev, *Forensci. Sci. Int.* **2009**, *188*, 1.
[14] T. L. Guidotti, J. McNamara, M. S. Moses, *Indian J. Med. Res.* **2008**, *128*, 524.
[15] V. Sikirzhytski, K. Virkler, I. K. Lednev, *Sensors* **2010**, *10*, 2869.
[16] S. Hu, J. A. Loo, D. T. Wong, *Proteomics* **2006**, *6*, 6326.
[17] P. Salvo, F. Di Francesco, D. Costanzo, C. Ferrari, M. G. Trivella, D. De-Rossi, *IEEE Sens. J.* **2010**, *10*, 1557.
[18] Y. Haixia, L. Dachao, R. C. Roberts, X. Kexin, N. C. Tien, *J. Microelectromech. Syst.* **2012**, *21*, 917.
[19] A. Lay-Ekuakille, S. Mukhopadhyay, S. Coyle, F. Benito-Lopez, R. Byrne, D. Diamond, in *Wearable and Autonomous Biomedical Devices and Systems for Smart Environment*, Vol. *75*, Springer-Berlin Heidelberg **2011**, 177.
[20] S. Coyle, K. T. Lau, N. Moyna, D. O'Gorman, D. Diamond, F. Di Francesco, D. Costanzo, P. Salvo, M. G. Trivella, D. E. De Rossi, N. Taccini, R. Paradiso, J. A. Porchet, A. Ridolfi, J. Luprano, C. Chuzel, T. Lanier, F. Revol-Cavalier, S. Schoumacker, V. Mourier, I. Chartier, R. Convert, H. De-Moncuit, C. Bini, *IEEE Trans. Inf. Technol. Biomed.* **2010**, *14*, 364.
[21] R. Badugu, J. Lakowicz, C. Geddes, *J. Fluoresc.* **2003**, *13*, 371.
[22] R. Badugu, J. R. Lakowicz, C. D. Geddes, *Anal. Chim.* **2003**, *76*, 610.
[23] L. Yu-Te, Y. Huanfen, A. Lingley, B. Parviz, B. P. Otis, *IEEE J. Solid-State Circuits* **2012**, *47*, 335.
[24] A. Caduff, M. S. Talary, M. Mueller, F. Dewarrat, J. Klisic, M. Donath, L. Heinemann, W. A. Stahel, *Biosens. Bioelectron.* **2009**, *24*, 2778.
[25] M. D. Larrañaga, Q. Wang, in *Patty's Toxicology*, John Wiley & Sons, Inc., Hoboken **2001**.
[26] B. Benelam, L. Wyness, *Nutr. Bull.* **2010**, *35*, 3.
[27] J. A. Mangos, N. R. McSherry, *Science* **1967**, *158*, 135.
[28] H. Suzuki, *Arch. Dermatol. Res.* **1998**, *290*, 523.
[29] S. Bhadra, G. E. Bridges, D. J. Thomson, M. S. Freund, *J. Nanotechnol. Eng. Med.* **2011**, *2*, 011011.
[30] M. A. Fonseca, J. M. English, M. von Arx, M. G. Allen, *J. Microelectromech. Syst.* **2002**, *11*, 337.
[31] T. J. Harpster, B. Stark, K. Najafi, *Sens. Actuators, A* **2002**, *95*, 100.
[32] R. Nopper, R. Niekrawietz, L. Reindl, *IEEE Trans. Instrum. Meas.* **2010**, *59*, 2450.
[33] C. Cametti, S. Marchetti, C. M. C. Gambi, G. Onori, *J. Phys. Chem. B* **2011**, *115*, 7144.
[34] P. G. Agache, C. Monneur, J. L. Leveque, J. Rigal, *Arch Dermatol Res.* **1980**, *269*, 221.
[35] R. Pelrine, R. Kornbluh, J. Joseph, R. Heydt, Q. Pei, S. Chiba, *Mater. Sci. Eng. C* **2000**, *11*, 89.
[36] N. Fries, *Capillary Transport Processes in Porous Materials: Experiment and Model,* Cuvillier Verlag, Göttingen 2010.
[37] S. P. Sutera, R. Skalak, *Annu. Rev. Fluid Mech.* **1993**, *25*, 1.
[38] E. Strommer, M. Hillukkala, A. Ylisaukko-oja, in *Wireless Sensor and Actor Networks*, Vol. *248*, Springer, Berlin Heidelberg **2007**, 131.
[39] E. Kehoe, R. L. Penn, *J. Chem. Educ.* **2013**, *90*, 1191.

Received: February 21, 2014
Revised: March 13, 2014
Published online: April 6, 2014

